Algorithm to Calculate Sliding Velocities for Spherical Roller Bearings

Slavomír Hrček[1](✉), Róbert Kohár[1], Michal Lukáč[1], Ján Šteininger[2], and Jozef Jenis[1]

[1] University of Žilina, Univerzitná, 8215/1, 01026 Žilina, Slovakia
slavomir.hrcek@fstroj.uniza.sk
[2] Institute of Competitiveness and Innovations, Univerzitná, 8215/1, 01026 Žilina, Slovakia

Abstract. The excellent operating properties of the mechanisms are conditioned by the quality design of the geometry of the individual components. Roller and ball bearings, which are frequently used components, have no exception and are an important part of them. One of the important parameters for a geometry design of antifriction bearings elements is sliding velocity. This article discusses the proposed algorithm for calculating sliding velocities between rolling elements and raceways of spherical roller bearings. Sliding velocities caused by different rolling radii along the rolling element profile and thus adversely effect of their abrasion. Using this algorithm can be quantified these adverse effects and the internal geometry of the spherical roller bearings can be modified to minimize the impact of sliding velocities. For this experimental study, a fully parametric 3D virtual model of spherical rolling bearings was created in the PTC/Creo Parametric CAD system and a FEM analysis was done in Ansys/Workbench CAE software. This work was done at University of Žilina, Faculty of Mechanical Engineering, Department of Design and Machine Elements.

Keywords: Spherical Roller Bearings · Sliding Velocities · Algorithm · FEM

1 Introduction

Ball and roller bearings were historically called antifriction bearings because of the low friction properties associated with them. Actually, the major portion of friction associated with rolling bearings is caused by sliding motions in the contacts between components. Contacts between components, which are rolling elements and raceways, rolling elements and cage, roller ends and roller guide flanges, and cage rails, and inner or outer ring lands [1]. Rolling element bearings are typical tribological components. They utilize low frictional rolling contacts between rolling elements and raceways to support load while permitting constrained and low resistant motion of one body relative to another [2]. One component that causes friction between the roller and the raceways is the sliding velocities that occur when the rolling radii along the roller bodies are too different. This article discusses the proposal of an algorithm to determine sliding velocities for rolling bearings [1].

J. Homišin et al. (Eds.): ICMD 2020, AHE 17, pp. 158–170, 2023.
https://doi.org/10.2991/978-94-6463-182-1_18

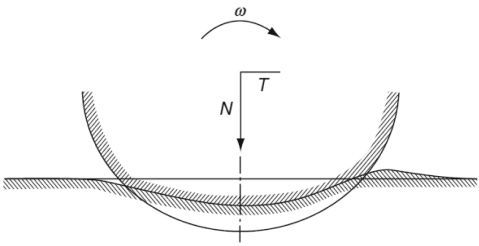

Fig. 1. Roller–raceway contact showing bulge due to rolling deformation [1].

1.1 Deformation

The balls or rollers in a bearing are mainly subjected to loads perpendicular to the tangent plane at each contact surface. Because of these normal loads, the rolling elements and raceways are deformed at each contact, producing according to Hertz, a radius of curvature of the common contacting surfaces equal to the harmonic mean of the radii of the contacting bodies. For a roller of diameter D, bearing on a cylindrical raceway of diameter di, the radius of curvature of a contact surface is

$$R = \frac{d_i D}{d_i + D} \tag{1}$$

Because of the deformation indicated above and because of the rolling motion of the roller over the raceway, which requires a tangential force to overcome rolling resistance, raceway material is squeezed up to form a bulge in the forward portion of the contact as shown in Fig. 1.

A depression is subsequently formed in the rear of the contact area. Thus, an additional tangential force is required to overcome the resisting force of the bulge. The bulge is very small and the friction force is insignificant [1].

1.2 Elastic Hyteresis

As may be observed in the discussion, as a rolling element under compressive load travels over a raceway, the material in the forward portion of the contact in the direction of rolling undergoes compression while the material in the rear of the contact is relieved of stress. It is recognized that as load is increasing, a given stress corresponds to a smaller deflection than when load is de creasing. The area between the curves (see Fig. 2) is called the hysteresis loop, and it represents an energy loss (friction power loss).

Generally, friction due to elastic hysteresis is very small compared with other types of friction occurring in rolling bearings [1].

In [1, 3] is mentioned that Drutkowsky verified this by experimenting with balls rolling between flat plates. Friction coefficients as low as 0.0001 is for 12.7 mm chrome steel balls rolling on chrome steel plates under normal loads of 356 N. In [4] Greenwood evaluated the rolling resistance due to elastic hysteresis. They found that the frictional resistance is substantially less than that due to sliding if the normal load is sufficiently large.

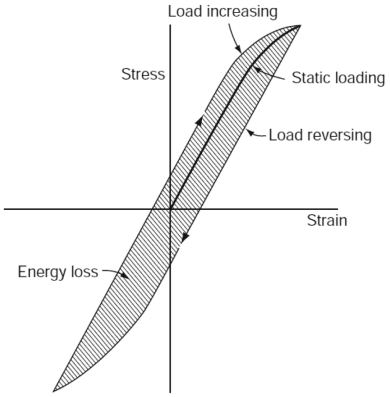

Fig. 2. Hysteresis loop for elastic material subjected to reversing stresses [1].

Drutkowski in [5] also demonstrated the linear dependence of rolling friction on the volume of stressed material. In [3, 5] Drutkowski showed the dependence of elastic hysteresis on the material under stress and the specific load on the contact area.

1.3 Microslip

If a radial cylindrical roller bearing had rollers and raceways of exactly the same lengths, if the rollers were accurately guided by frictionless flanges, and if the bearing operated with zero misalignment under moderate speed, then gross sliding in the roller–raceway contacts would not occur. Gross sliding refers to the total slip of one surface over another. Depending on the elastic properties of the contacting bodies and the coefficient of friction between the contacting surfaces, microslip could occur. The coefficient of friction can be defined as the ratio of the tangential force F to the normal force Q (see Fig. 3). Microslip is defined as the partial sliding of one surface relative to the other:

$$\mu = \frac{F}{Q} \tag{2}$$

In [5], Reynolds first referred to microslip when, in his experiments involving rolling of an elastically stiff cylinder on rubber, he observed that since the rubber stretched in the contact zone, the cylinder rolled forward a distance less than its circumference in one complete revolution about its axis. This experiment was conducted in the absence of a lubricating medium, that is, dry contact.

Poritsky in [6] demonstrated the microslip or creep phenomenon in two dimensions considering the action of a locomotive driving wheel, also dry contact. The normal load between contacting cylinders was assumed to generate a parabolic stress distribution, similar to a Hertzian stress distribution, over the contact surfaces (see Fig. 3).

Superimposed on this stress distribution with stresses σ_z was a tangential stress τ_x. In this case, the local coefficient of friction in the contact is

$$\mu_x = \frac{\tau_x}{\sigma_z} \tag{3}$$

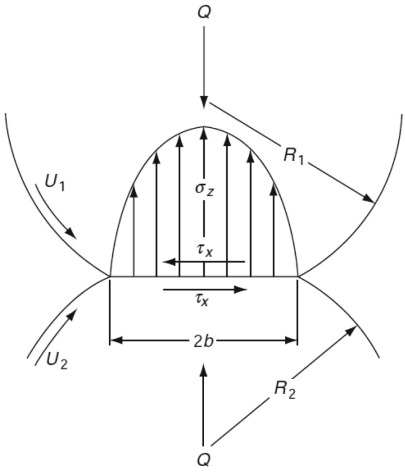

Fig. 3. Rolling under action of surface tangential stress [1].

Using this model, Poritsky demonstrated the existence of a "locked" region over which no slip occurs and a region of relative movement or slip over a contact area for which it was historically assumed that only rolling occurred. This is illustrated in Fig. 4. Cain in [8] further determined that in pure rolling the locked region coincided with the leading edge of the contact area. It must be emphasized that the locked region can only occur when the friction coefficient is very high as between two unlubricated surfaces.

In [9] is determined that a hard ball rolling in a closely conforming groove can roll without sliding only on two narrow bands. Ultimately, Heathcote obtained a formula for the rolling friction in this situation. While Heathcote slip is very similar to that which occurs because of rolling element–raceway deformation, Heathcote's analysis takes no account of the ability of the surfaces to elastically deform and accommodate the difference in surface velocities by differential expansion.

In [1] is mentioned that Johnson, expanded on the Heathcote analysis by slicing an elliptical contact area, such as that in a ball–raceway contact, into differential slabs of area as shown in Fig. 5 and thereafter applying the Poritsky analysis for each slab. Johnson's analysis using elastic tangential compliance demonstrates a lower coefficient of friction; this assumes sliding rather than microslip. The Fig. 6 shows the locked and slip regions that obtain within the contact ellipse.

1.4 Sliding Friction

Friction force parallel to the rolling direction is calculated by integrating over the contact area from -*a* to + *a* and -*b* to + *b*. Let think $q = x/a$ and $t = y/b$:

$$F_y = \frac{3\mu Q}{2\pi ab}\int_{-1}^{+1}\int_{-\sqrt{1-q^2}}^{+\sqrt{1-q^2}}\left(1-q^2-t^2\right)^{1/2} dt\, dq \tag{4}$$

where the sliding velocity direction coefficient, is + 1 or -1 depending on the direction of sliding.

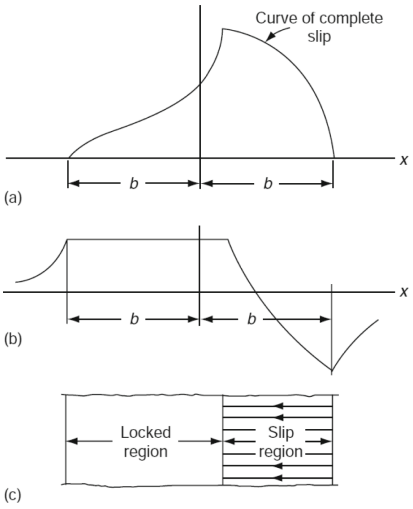

Fig. 4. Surface tangential actions; (b) surface strains; (c) locked and microslip regions [1].

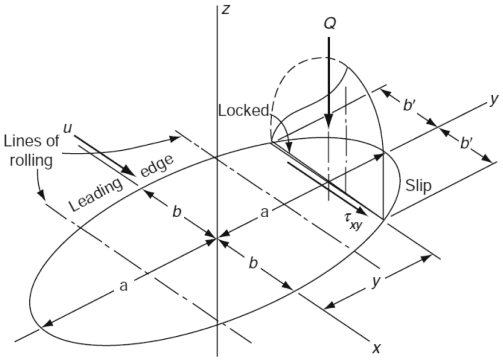

Fig. 5. Ball–raceway contact ellipse showing locked region and microslip region radial ball bearing [1].

Equation 4 is valid for operating conditions involving solid-film lubrication and boundary lubrication where friction coefficient μ can be characterized as a constant [1].

1.5 Overall Surface Friction Shear Stress

When the lubricant film is insufficient to completely separate the surfaces in rolling contact, that is for $\Lambda < 3$, some of the surface peaks, also called asperities, as illustrated in Fig. 7, break through the lubricant film and contact each other. The sliding friction shear stress during this asperity–asperity interaction occurs in the regime of boundary lubrication and may be calculated using Eq. 4 for a ball–raceway or point contact [1].

Only a portion of the contact, however, operates in this manner; the remainder of the contact surface operates according to fluid-film lubrication [1].

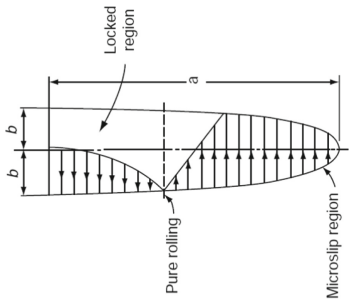

Fig. 6. Surface tangential actions; (b) surface strains; (c) locked and microslip regions [1].

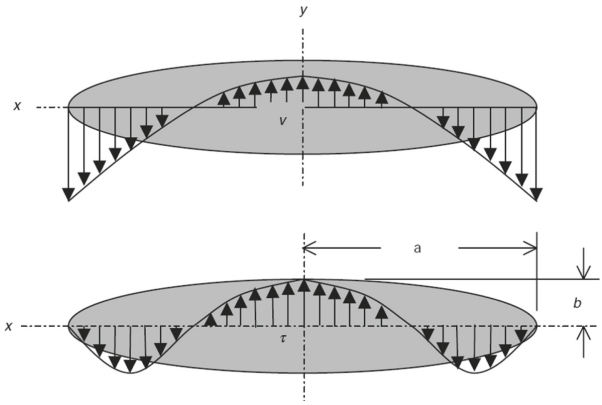

Fig. 7. Distributions of sliding velocity and surface friction shear stress over an elliptical area of rolling element–raceway contact in a radially loaded, radial ball bearing [1].

2 Materials and Methods

2.1 Proposal of Algorithm for Calculation Sliding Velocity

The using of many advanced software tools are needed for calculation of sliding velocity in rolling bearings. The loading determines real deformation and then the real rolling radii include these deformations. The proper FEA software need to be used for determination. The inner geometry of rolling bearing is too complicated. Therefore, a useful CAD tool is recommended to use. Via this CAD tool should be possible also work with parametric model. The FEA analysis results and mathematical calculations have to be evaluated. We used origin script for results evaluation, which one has been created in useful programming language. The Fig. 8 shows the algorithm for calculation of the sliding velocities in rolling bearings.

2.2 Application of Algorithm at Spherical Roller Berings

Virtual Model of Spherical Rolling Bearing. For FEM analysis, a fully parametric 3D virtual model of spherical rolling bearings was created in the PTC/Creo Parametric CAD

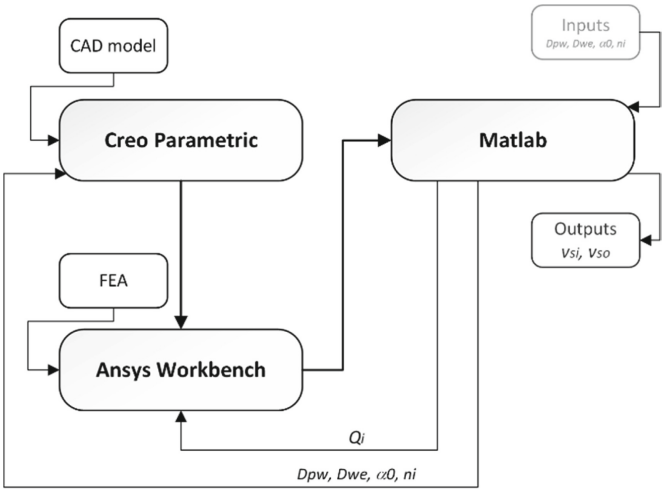

Fig. 8. Algorithm to calculate sliding velocities.

system. This model was designed so that its geometry was controlled by the parameters through relations. In this way, we were able to efficiently modify individ-ual dimensions and create size-based series of spherical rolling bearings. The Fig. 9 shows a view with the control parameters [10]

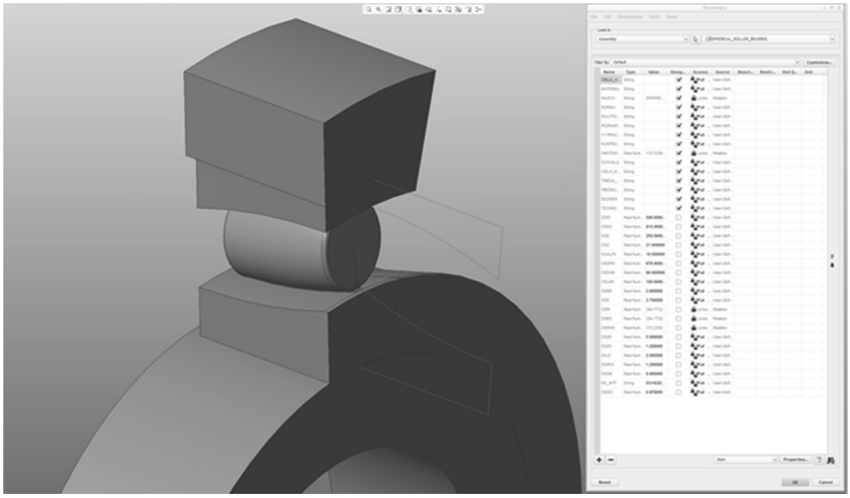

Fig. 9. Virtual model of spherical rolling bearings [10].

2.3 FEM Analysis

In order to perform FEM analysis, we used Ansys/Workbench CAE software, in which we defined static structural analysis for the spherical rolling bearing model. The resulting virtual 3D model of a spherical rolling bearing was imported from the PTC/Creo Parametric system via an interface to the Ansys/Workbench environment. This interface enables us to modify the parameters and thus change the rolling bearing model directly from the Ansys/Workbench environment.

For all spherical rolling bearing components we used a linear isotropic elasticity material model with Young's modulus $E = 210\ 000\ MPa$ and Poisson's ratio $\mu = 0.3$ for bearing steels. We chose a linear material model because we applied such maximum radial load Fr acting on the spherical rolling bearing that we would avoid exceeding the yield strength of the material and the maximum contact pressure exceeding $p_o = 3\ 500\ MPa$, which is defined as the threshold value for line contact.

Symmetry was applied to the model in one plane X-Y for reducing the computational time. The model mesh (see Fig. 10) was created by standard elements from the Ansys library. The volume mesh was created with the SOLID185 element. Individual bearing elements are in contact because the forces acting upon the bearing are transferred between rings (their raceways) and roller. Elements type CONTA174 and TARGE170 were used for mesh contact pairs (rolling elements – raceways). Choosing an appropriate mesh element size is necessary in order to correctly analyze the contact pressure between the roller and raceway of the outer and inner rings.

The contacts between the rolling elements and orbital paths of the two rings (races) were defined as frictionless type.

The loading in radial direction is applied on shaft. The boundary condition – Displacement in X-axis is defined against axial movement of bearing rings. Displacement in Y-axis is defined opposite of radial load force (see Fig. 11).

The result of FEM analysis is the distribution of contact pressure and the deformations of raceway of bearing rings and roller in contact area.

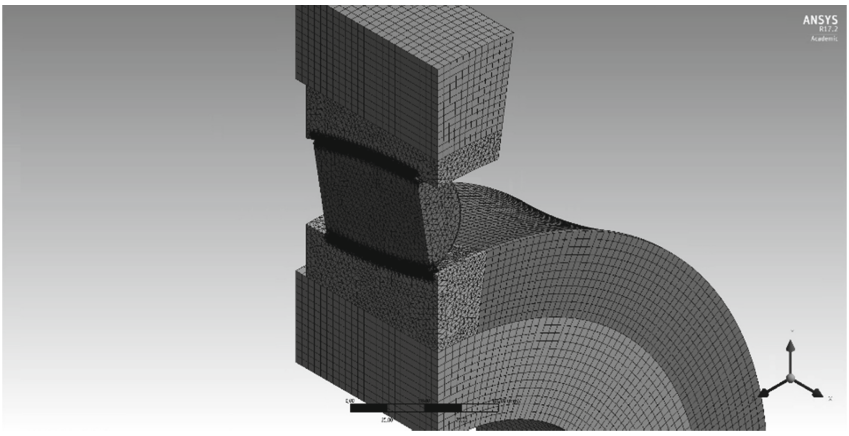

Fig. 10. FEM model of spherical rolling bearings.

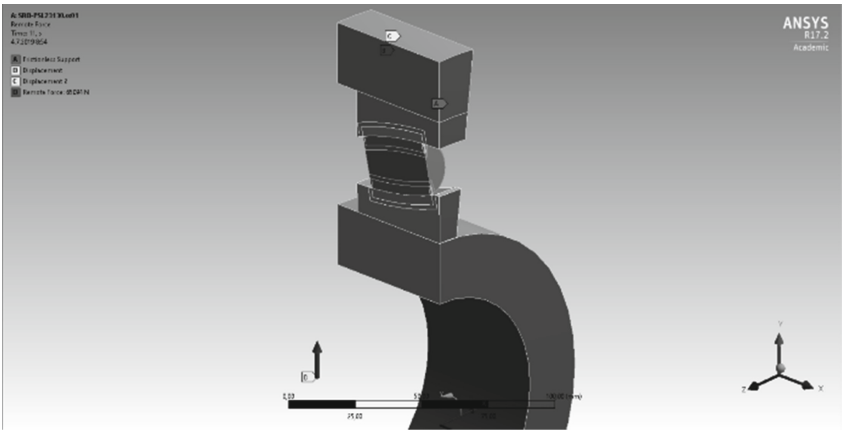

Fig. 11. Boundary conditions and load applied on FEA model SRB.

3 Results and Discussing

3.1 Processing Results from FEM Analysis

The deformations, which are evaluated by Ansys are not the true deformation. In this case we are talking about complex movement of nodes/elements. This complex movement includes body movement (e.g. due to close gap) and contact stiffness and true deformation. This is the reason why the subsequently evaluation of these results is still needed for determination of the true deformation. The origin script in Matlab was created for results evaluation. Output of this script is calculation of the true deformation of raceways for inner ring and roller (see Fig. 12) and true deformation of raceway for outer ring and roller (see Fig. 13).

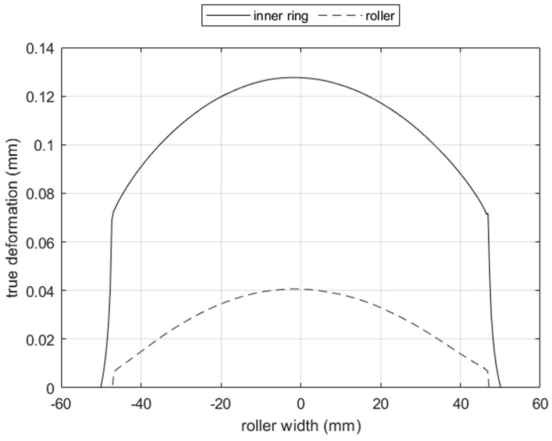

Fig. 12. True deformation on roller and raceway of the inner ring.

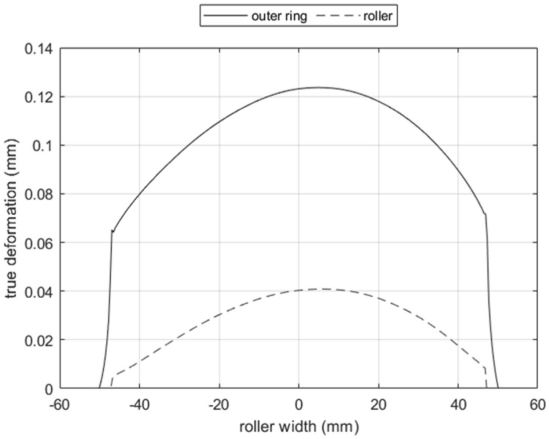

Fig. 13. True deformation on roller and raceway of the outer ring.

3.2 Calculating Zero Sliding Velocity Distance

For rolling bearings with curved surfaces, pure rolling can occur at most at two points in the contact area. If spinning is absent at a raceway contact, then all points on lines parallel to the direction of rolling and passing through the aforementioned points of pure rolling roll without sliding. Distribution of sliding velocity on the contact surface is illustrated in Fig. 14. The lines of pure rolling lie at $x = \pm ca$.

Using Eq. 4 to describe the differential frictional force dF, it can be seen that the net sliding frictional force in the direction of rolling at a raceway contact is

$$F_y = \pm\frac{3\mu Q}{\pi ab}\left\{\int_0^{ca}\int_{-\sqrt{1-q^2}}^{+\sqrt{1-q^2}}\left(1-q^2-t^2\right)^{1/2}dt\,dq - \int_{ca}^{a}\int_{-\sqrt{1-q^2}}^{+\sqrt{1-q^2}}\left(1-q^2-t^2\right)^{1/2}dt\,dq\right\} \tag{5}$$

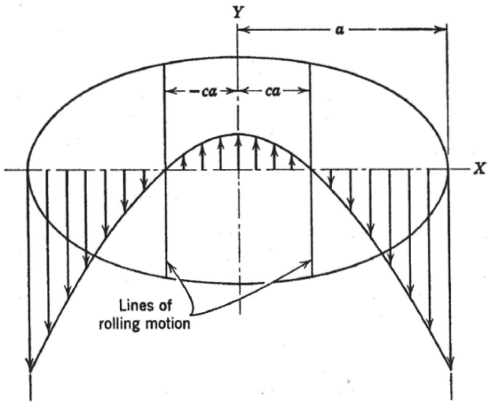

Fig. 14. Distribution of sliding velocity on the elliptical contact surface for negligible gyroscopic motion and zero spin.

Using the integral, in Eq. (5) is possible calculate the distance ca where is the pure rolling without slip. For this purpose was created a script in Matlab for this calculation using a nonlinear solver.

3.3 Calculation of Sliding Velocity at Spherical Roller Bearing

Spherical roller bearings with curved raceways and crowned rollers will be permit slippages during rolling over the width of the contact surfaces due to unequal rolling radii (see Fig. 15). These sliding velocities adversely affect the abrasion on surfaces of the roller and the raceways of the bearing rings.

Sliding velocities between the rolling element and the raceways are calculated from the true rolling radii and angular velocities at the points with pure rolling without slip. To calculate the angular velocities, the relationships for calculating the planetary gear can be used, where the inner ring corresponds to a sun gear, the outer ring corresponds to the ring gear, the carrier is the cage and the satellites are rolling elements. For a rotating inner ring, Eq. 6 applies to the calculation of the sliding velocities between the inner ring and the roller and Eq. 7 applies to calculate the sliding velocity between the roller and the outer ring.

$$v_i = \omega_r \cdot r_r - (\omega_c - \omega_i) \cdot r_i \tag{6}$$

$$v_o = \omega_r \cdot r_r + \omega_c \cdot r_o \tag{7}$$

where v_ι is sliding velocity between roller and raceway of the inner ring; v_o is sliding velocity between roller and raceway of the outer ring; ω_r is angular velocity of roller; ω_c is angular velocity of cage/carrier; ω_i is angular velocity of inner ring; r_r is true rolling radius of roller, r_i is true rolling radius of the inner ring raceway; and r_o is true rolling radius of the outer ring raceway.

The proposed algorithm was used to calculate sliding velocities between the raceways and the rolling element shown in Fig. 16. Dimensions of bearing are pitch diameter: $d_{pw} = 678\ mm$, roller diameter: $d_{we} = 80\ mm$, roller length: $l_{we} = 100\ mm$, nominal contact angle*:* $a_0 = 10.5°$, revolution of inner ring: $n_i = 100\ rpm$, radial load: $Q_{max} = 1\ 430\ kN$.

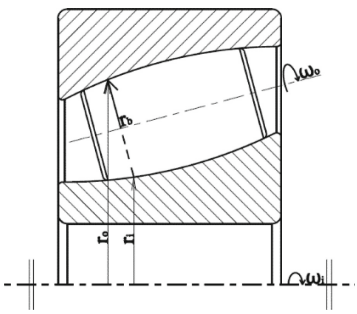

Fig. 15. Real rolling radius of the spherical roller bearing.

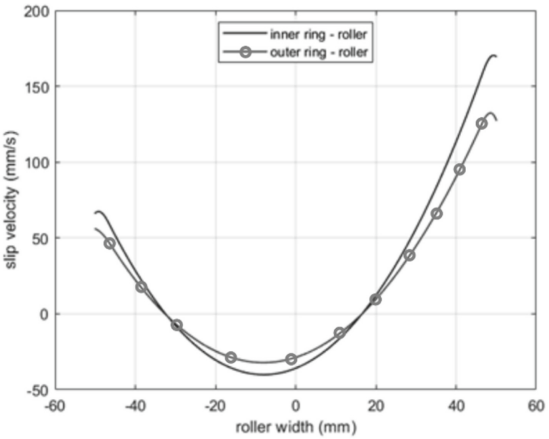

Fig. 16. Calculated sliding velocities for a SRB bearing at the given load.

4 Conclusions

By the present algorithm, it is possible to calculate the sliding velocities between the rolling elements and the raceways of the bearing rings in practically any type of rolling bearing. Its use is most important for bearings that have a larger nominal contact angle and large differences in orbit radii. Spherical roller bearings are the biggest sufferers.

By the proposed algorithm, it is possible to solve the influence of the internal rolling bearing geometry on the resulting sliding velocities, which adversely affect the abrasion of the rolling elements and the raceways of the bearing rings. These abrasions can cause premature failure of the rolling bearing. The proposed algorithm is an effective tool in the design process of rolling bearing geometry at early stages of their development. It requires the use of modern software tools, with which sliding velocities can be calculated using the proposed algorithm.

Acknowledgement. This work was supported by Ministry of Education, Science, Research and Sport under the contract No. 1/0595/18 – Optimising the internal geometry of roller bearings with line contact in order to increase their durability and reduce their structural weight. This work was supported by Grant system of the University of Žilina.

References

1. Harris, T., A., Kotzalas, M., N.: Advanced Concepts of Bearing Technology. 1st edn. Taylor & Francis Group (2007).
2. Ai, X.: Function and Structure of Rolling Element Bearings. In: Wang Q.J., Chung YW. (eds) Encyclopedia of Tribology. Springer, Boston, MA (2013).
3. Drutowski, R.: Energy losses of balls rolling on plates, Friction and wear. Elsevier, Amsterdam, pp. 16–35 (1959).

4. Greenwood, J., Tabor, D.: The friction of hard sliders on lubricated rubber: The importance of deformation losses. Proc. Phys. Soc. London, 71, 989 (1958).
5. Drutowski, R. Linear dependence of rolling friction on stressed volume, Rolling contact phenomena, Elsevier, Amsterdam (1962).
6. Reynolds, O.: On rolling friction. Philos. Trans. R. Soc. London, 166, pp. 155-174 (1875).
7. Poritsky, H., J.: Stress and deflexions of cylindrical bodies in contact with application to contact of gears and of locomotive wheels. Appl. Mech., 72, 191–201 (1950).
8. Cain, B., J.: Discussion: "Stresses and deflections of cylindrical bodies in contact with application to contact of gears and of locomotive wheels. Appl. Mech., 72, 465 (1950).
9. Heathcote, H.: The ball bearing. Proc. Inst. Automob. Eng., London, 15, 569 (1921).
10. Madaj, R., Kohar, R.: Support tools in the development of bearings for wind turbines. In: Dynybyl V., Berka, O., Petr, K., Lopot, F., Dub, M. (eds) Latest Methods of Construction Design. 55th International Conference of Machine Design Departments. Prague, Czech Republic. pp 57–62. Springer, Cham (2016).